Cancer Research

MSH2 Dysregulation Is Triggered by Proinflammatory Cytokine Stimulation and Is Associated with Liver Cancer Development

Yuji Eso[1], Atsushi Takai[1], Tomonori Matsumoto[1], Tadashi Inuzuka[1], Takahiro Horie[2], Koh Ono[2], Shinji Uemoto[3], Kyeryoung Lee[4], Winfried Edelmann[4], Tsutomu Chiba[1], and Hiroyuki Marusawa[1]

Abstract

Inflammation predisposes to tumorigenesis in various organs by potentiating a susceptibility to genetic aberrations. The mechanism underlying the enhanced genetic instability through chronic inflammation, however, is not clear. Here, we demonstrated that TNFα stimulation induced transcriptional downregulation of *MSH2*, a member of the mismatch repair family, via NF-κB–dependent miR-21 expression in hepatocytes. Liver cancers developed in *ALB-MSH2*$^{-/-}$*AID*$^{+}$, *ALB-MSH2*$^{-/-}$, and *ALB-AID*$^{+}$ mice, in which *MSH2* is deficient and/or activation-induced cytidine deaminase (*AICDA*) is expressed in cells with albumin-producing hepatocytes. The mutation signatures in the tumors developed in these models, especially *ALB-MSH2*$^{-/-}$*AID*$^{+}$ mice, closely resembled those of human hepatocellular carcinoma. Our findings demonstrated that inflammation-mediated dysregulation of *MSH2* may be a mechanism of genetic alterations during hepatocarcinogenesis. *Cancer Res; 76(15); 4383–93. ©2016 AACR.*

Introduction

It is well established that chronic inflammation predisposes to tumor development in various organs, including hepatitis virus–associated hepatocellular carcinoma (1, 2). On the other hand, cancer cells are considered to be generated by a stepwise accumulation of genetic alterations in various tumor-related genes during the process of tumorigenesis (3–5). Thus, the genetic aberrations required for malignant transformation could be accumulated in nontumorous inflamed tissues with a high risk of tumorigenesis. Indeed, whole-exome sequencing has revealed many somatic mutations in various genes in hepatitis C virus (HCV)-infected cirrhotic liver tissues (6). Accumulation of various somatic mutations in nontumorous epithelial cells has also been reported in other tissues with chronic inflammation (7, 8). These data indicate that chronic inflammation potentiates a susceptibility to gene alterations during carcinogenesis. However, the precise mechanisms underlying the generation of genetic alterations during inflammation-associated carcinogenesis remain largely unknown.

Recent advances in sequencing technology revealed the landscape of genetic aberrations in human cancers (9). The abundant information on mutation signatures in various cancers provides a clue to the molecular processes involved in genetic aberrations during carcinogenesis. Interestingly, recent studies have shown that mutation signatures detected in several human cancer tissues exhibit the conserved footprints of the activity of nucleotide-editing enzymes, the APOBEC family proteins (10, 11). Among the APOBEC family members, activation-induced cytidine deaminase (AID) is a well-defined molecule capable of inducing mutations in human DNA sequences, including immunoglobulin gene (12). We previously demonstrated that aberrant expression of AID is induced in response to inflammatory conditions and contributes to tumorigenesis through production of somatic mutations during carcinogenesis, including hepatocellular carcinoma and gastric cancers (13–17). Consistently, a strong preference for C:G to T:A transition mutations, a typical footprint of AID, is observed in the mutation signature of both *Helicobacter pylori*–associated gastric cancer and HCV-associated hepatocellular carcinoma (6, 7).

On the other hand, DNA mismatch repair (MMR) system plays a critical role in maintaining genomic stability, and indeed, it protects the genome against the mutagenic activity of AID (18). Consistently, C:G to T:A footprints of cytidine deaminase–mediated nucleotide alterations could be unmodified and well conserved under MMR-deficient conditions (19). Thus, it is reasonable to assume that high incidence of C:G to T:A transition mutations observed in various human inflammation–associated cancers may involve dysfunction of MMR. In this study, therefore, we examined whether inflammation induces dysregulation of MMR and, if so, its role in inflammation-associated carcinogenesis.

[1]Department of Gastroenterology and Hepatology, Graduate School of Medicine, Kyoto University, Kyoto, Japan. [2]Department of Cardiovascular Medicine, Graduate School of Medicine, Kyoto University, Kyoto, Japan. [3]Department of Surgery, Graduate School of Medicine, Kyoto University, Kyoto, Japan. [4]Department of Cell Biology, Albert Einstein College of Medicine, Bronx, New York.

Note: Supplementary data for this article are available at Cancer Research Online (http://cancerres.aacrjournals.org/).

Corresponding Author: Hiroyuki Marusawa, Department of Gastroenterology and Hepatology, Graduate School of Medicine, Kyoto University, 54 Kawahara-cho, Syogoin, Sakyo-ku, Kyoto 606-8507, Japan. Phone: 81-75-751-4319; Fax: 81-75-751-4303; E-mail: maru@kuhp.kyoto-u.ac.jp

doi: 10.1158/0008-5472.CAN-15-2926

Materials and Methods

Cell culture and transfection

Human hepatoma-derived cell lines, HepG2, Huh-7.5, and Hep3B cells, were obtained from Institute for Virus Research, Kyoto University (Kyoto, Japan). All these cells were authenticated by short-tandem repeat analysis in January 2016 at JCRB Cell Bank, National Institute of Biomedical Innovation (Osaka, Japan). Cells were cultured in DMEM (Gibco by Life Technologies) supplemented with 10% FBS at 37°C in a humidified atmosphere with 5% CO_2. For transfection with plasmid DNA, Trans-IT LT1 Transfection Reagent (Mirus Bio Corporation) was used according to the manufacturer's protocol.

Reagents

Recombinant human TNFα was purchased from Peprotech EC. NF-κB inhibitory reagents SN50 and MG132 were purchased from Biomol International LP. Anti-MSH2/AFP antibody and anti-α-tubulin antibody were purchased from Santa Cruz Biotechnology and EMD Millipore, respectively. Anti-miR-21 inhibitor (anti-hsa-miR-21-5p miScript miRNA inhibitor) was purchased from Qiagen.

Plasmids

pcDNA3-IκBαΔN, plasmid for expression of the "super-repressor" form of the IκB-α protein, was described previously (14). Expression vectors for the negative control and miR-21 were generated using BLOCK-iT Pol II miR RNAi Expression Vector Kits following the manufacturer's protocol (Life Technologies). To create the anti-miR-21 "decoy" vector, the luciferase 3′-untranslated lesion was modified to include three tandem sequences complementary to miR-21, separated by two nucleotide spacers. The construct was analyzed using an ABI 3500 Genetic Analyzer and correctly inserted into a pLenti6/V5-D-TOPO vector (Life Technologies) driven by a CMV promoter to stably express genes in hepatocytes.

RNA extraction and qRT-PCR for mRNA

Total RNA was isolated and purified using Sepasol-RNA 1 Super (Nacalai Tesque) according to the manufacturer's protocol. cDNA was synthesized from 1 μg total RNA using the Transcriptor High Fidelity cDNA Synthesis Kit (Roche) in accordance with the manufacturer's instructions. Quantification of gene expression was performed by real-time RT-PCR using the LightCycler 480 Real-Time PCR System (Roche). To assess the quantity of isolated RNA as well as the efficiency of cDNA synthesis, target cDNAs were normalized to the expression level of endogenous mRNA of the "housekeeping" reference 18S rRNA (15). Each sample was tested in triplicate. Gene-specific primers are shown in Supplementary Table S1.

Quantitative PCR for miRNAs

Total RNA was isolated using Sepasol-RNA 1 Super (Nacalai Tesque) according to the manufacturer's protocol. miR-21 expression levels were assessed in accordance with the TaqMan MicroRNA Assays (Life Technologies) protocol, and the products were analyzed using the LightCycler 480 Real-Time PCR System (Roche). miR-21 expression levels were normalized by U6 small nuclear RNA expression. Each sample was tested in triplicate.

Western blotting

For immunoblotting analysis, cells were lysed in RIPA buffer with protease inhibitor, and lysates were centrifuged at 12,000 rpm for 15 minutes at 4°C to remove cellular debris. Supernatants were diluted in SDS-PAGE sample buffer and boiled at 70°C for 10 minutes. Protein samples were separated using 7.5% Mini-PROTEAN TGX Precast Gels (Bio-Rad Laboratories) according to the manufacturer's instructions and transferred to polyvinylidene difluoride membranes. The membranes were blocked with Block Ace Powder (DS Pharma Biomedical), diluted in PBS containing 0.05% Tween 20 (Sigma-Aldrich) overnight at 4°C, and incubated with primary antibody (anti-MSH2, 1:200; anti-α-tubulin, 1:200 dilution) for 1 hour. Following a washing step in PBS-0.05% Tween 20 (0.05% PBST), the membranes were incubated with secondary antibody (Bio-Rad Laboratories; anti-rabbit IgG, 1:3,000; anti-mouse IgG, 1:3,000 dilution) for 30 minutes. The membranes were then washed in 0.05% PBST and detected by Immobilon Western Chemiluminescent HRP Substrate (Millipore Corporation) using the LAS-3000 system (FujiFilm).

Lentivirus production and DNA transduction

Lentiviral stocks were produced in 293T cells in accordance with the manufacturer's protocol (Life Technologies). In brief, virus-containing medium was collected 48 hours posttransfection and filtered through a 0.45-μm filter. One round of lentiviral infection was performed by replacing the medium with virus-containing medium, followed by centrifugation at 2,500 rpm for 30 minutes at 30°C. Cells were used for analysis 3 days after transduction.

IHC

For histologic analysis, organs were fixed overnight in 10% formalin, paraffin-embedded, and sectioned at a thickness of 6 μm. Sections were then deparaffinized in xylene and rehydrated in graded ethanol. Before incubation, sections were autoclaved for 20 minutes at 121°C in Target Retrieval Solution (Dako) and soaked in blocking solution for 30 minutes. Later, sections were incubated in anti-MSH2-antibody or anti-AFP-antibody (1:200 dilution) at 4°C overnight and washed three times with PBS, then incubated with biotinylated anti-rabbit or goat IgG antibody (1:200 dilution; Vector Laboratories) for 30 minutes at 25°C. ABC reagent (avidin-biotinylated enzyme complex; Vector Laboratories) was added, and sections were incubated with 3.3-diaminobenzine tetrahydrochloride substrate (Vector Laboratories) until the desired stain intensity developed.

Dual-luciferase assays

Luciferase activities were measured using the Dual-Luciferase Reporter Assay System (Promega Corp.) following the manufacturer's protocol. The relative luciferase activity of each construct is reported as the fold induction.

Mice

The *Msh2*$^{LoxP/LoxP}$ mice (20) on a C57BL/6 background were a gift from Dr. Winfried Edelmann (Albert Einstein College of Medicine, Bronx, New York) and maintained in a specific pathogen-free facility at Kyoto University Faculty of Medicine (Kyoto, Japan). The *AID cTg* mice (21) were deposited at the Riken Bioresource Center (Tsukuba, Japan; no. RBRC00892). The *ALB-Cre* mice (22) were a gift from the Center for iPS Cell Research

and Application, Kyoto University, and maintained by self-crossing between heterozygous mice. All mice were fed *ad libitum* and killed by cervical dislocation for censoring. Upon censoring, the numbers of macroscopic tumors were counted after laparotomy and thoracotomy. All animal experiments were approved by the Ethics Committee for Animal Experiments and performed under the Guidelines for Animal Experiments of Kyoto University.

Whole-exome capture and massively parallel sequencing

Fragmented DNA was used to prepare each DNA-sequencing library. The DNA libraries were prepared according to the instructions provided with the Ion Xpress Plus Fragment Library Kit (Life Technologies). Whole-exome sequence capture was then performed using SureSelect Mouse All Exon Kit (Agilent Technologies) according to the manufacturer's instructions. The captured samples were sequenced as 130-bp paired-end reads using the Ion Proton System (Life Technologies), and the data were converted to the FASTQ format.

Using NextGENe 2nd Generation Sequence Analysis Software v2.3.4.2 (SoftGenetics), the obtained reads were aligned with the Mouse Genome UCSC mm9. We identified somatic mutations using the strict variant filtering process (Supplementary Fig. S1). Sequence reads were deposited in the DNA data bank of Japan Sequence Read Archive (http://trace.ddbj.nig.ac.jp/dra/index_e.html) under accession number of DRA003790.

Human subjects

Human liver tissues with chronic HCV infection were obtained during curative resection of primary hepatocellular carcinoma at Kyoto University Hospital (Kyoto, Japan). As a control, normal liver tissues from patients with metastatic liver cancer were also examined. All information-identifying subjects were omitted. The Ethics Committee of Kyoto University Hospital approved analyses for human subjects, and written informed consent was obtained from all patients in accordance with the Declaration of Helsinki.

Statistical analysis

Data are expressed as means ± SE. Statistical comparisons were calculated using unpaired two-tailed Student *t* test or χ^2 test and Fisher exact test. A value of less than 0.05 was considered to indicate significance.

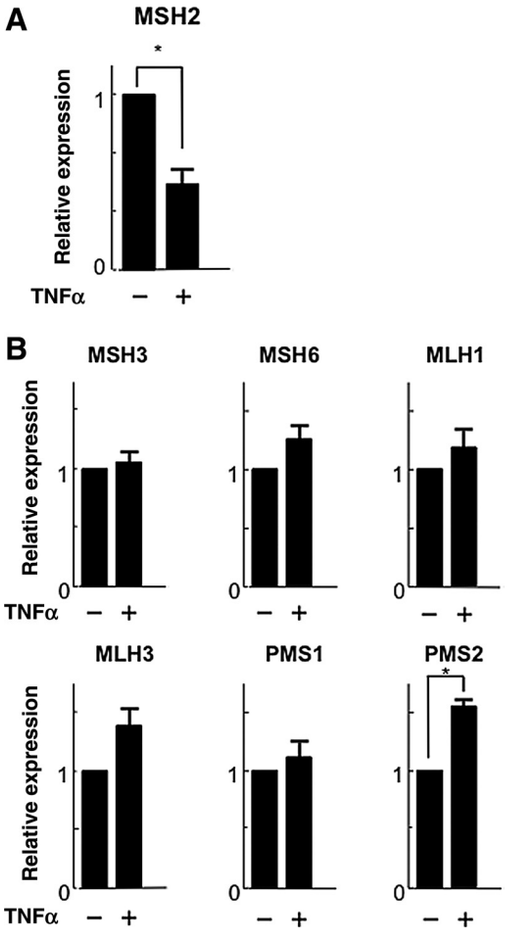

Figure 1.

MSH2 is downregulated in hepatocytes in response to TNFα stimulation. HepG2 cells were treated with or without TNFα (100 ng/mL) for 10 hours, and the expressions of MMR-related genes were measured by quantitative real-time RT-PCR. The expression level of each gene was normalized to *18S rRNA* as an endogenous control. **A,** the expression of *MSH2* was significantly reduced by TNFα stimulation. **B,** TNFα treatment induced no significant changes in the expression level of *MSH3, MSH6, MLH1, MLH3*, or *PMS1*. The expression of *PMS2* was significantly increased by TNFα stimulation (*, $P < 0.05$ vs. control).

Results

MSH2 is downregulated in response to proinflammatory cytokines via NF-κB signaling in human hepatocytes

The proinflammatory cytokine TNFα plays a central role in hepatic inflammation (23–25). Thus, we first examined the effects of TNFα on the expression of seven representative MMR-related genes in cultured human hepatocytes. Expression of all MMR-related transcripts examined was detected in quiescent HepG2 cells by quantitative real-time RT-PCR. Interestingly, among MMR-related genes, the expression of *MSH2* was significantly reduced after treatment with TNFα (Fig. 1A). In contrast, TNFα treatment resulted in significant upregulation of *PMS2*, and no significant changes in the expression of *MSH3*, *MSH6*, *MLH1*, *MLH3*, or *PMS1* (Fig. 1B). To further investigate the TNFα-mediated reduction of *MSH2*, we examined the time course of *MSH2* expression by incubating HepG2 cells with TNFα. *MSH2* expression was gradually reduced, and the lowest level was observed 6 hours after TNFα treatment (Fig. 2A). Moreover, TNFα reduced *MSH2* expression in a dose-dependent manner (Fig. 2B). To examine whether TNFα generally reduces *MSH2* expression in human hepatocytes, we analyzed *MSH2* expression in other hepatoma-derived cell lines, Huh-7.5 and Hep3B, and confirmed that treatment with TNFα significantly reduced *MSH2* expression in both types of cells (Fig. 2C). RT-PCR analysis revealed that *MSH2* transcripts also decreased in response to another proinflammatory cytokine, IL1β (Fig. 2D). Immunoblotting analyses confirmed that treatment with TNFα markedly downregulated MSH2 protein expression in both HepG2 and Huh-7.5 cells (Fig. 2E).

TNFα activates NF-κB and contributes to the regulation of various genes under inflammatory conditions (26). The findings that TNFα downregulates *MSH2* led us to examine whether *MSH2* expression is regulated in hepatocytes in an NF-κB–dependent manner. NF-κB inhibitory reagents, SN50 and MG132,

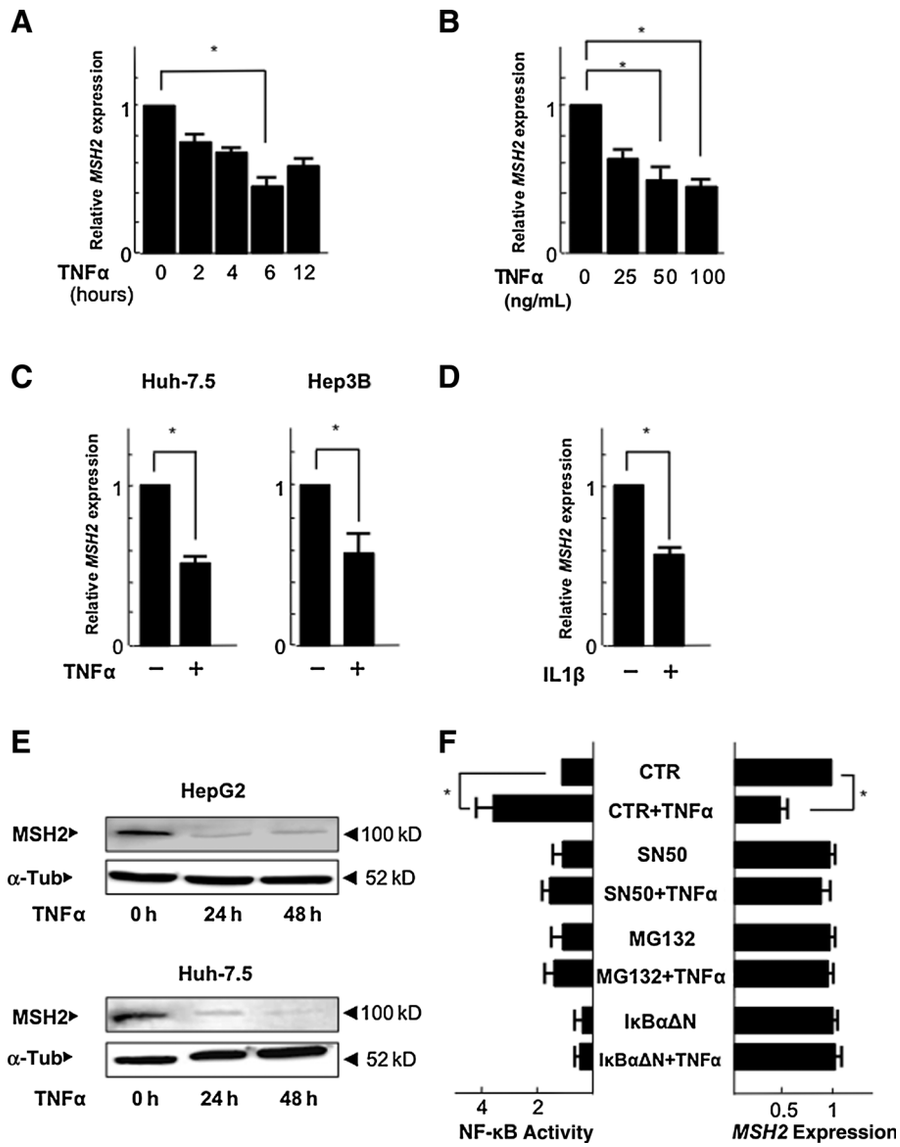

Figure 2.
MSH2 is downregulated in hepatocytes in response to proinflammatory cytokines via NF-κB signaling. **A** and **B,** time-dependent and dose-dependent (**B**) effects of TNFα on *MSH2* expression. HepG2 cells were treated with TNFα (100 ng/mL) at the indicated time points (**A**) or with various concentrations of TNFα (0–100 ng/mL) for 10 hours (**B**). **C,** Huh-7.5 and Hep3B cells were treated with TNFα (100 ng/mL) for 6 hours. **D,** HepG2 cells were treated with IL1β (25 ng/mL) for 10 hours. **E,** HepG2 and Huh-7.5 cells were treated with TNFα (100 ng/mL) for 0, 24, or 48 hours, followed by immunoblotting using anti-MSH2 antibody (top) or anti-α-tubulin antibody (α-Tub; bottom). **F,** effects of NF-κB inhibitors on TNF-α–induced NF-κB activity and *MSH2* expression. HepG2 cells were transfected with pNF-κB-Luc, followed by treatment with SN50 (50 μg/mL) or MG132 (2 μg/mL) for 2 hours, or transfected with pcDNA3-IκBαΔN, and further treated with TNFα (100 ng/mL) for 10 hours. Luciferase activity was monitored in each sample and normalized by the activity of *Renilla* luciferase (left bars). Total RNA was isolated from each sample, and *MSH2* expression levels were measured by quantitative real-time RT-PCR (right bars). *, $P < 0.05$ versus control.

significantly reduced TNFα-induced NF-κB activation, and pretreatment with either drug almost completely rescued the TNFα-induced *MSH2* downregulation (Fig. 2F). Furthermore, the *MSH2* downregulation induced by TNFα was almost completely rescued by coproduction of the superrepressor form of IκBα, a specific NF-κB inhibitor (Fig. 2F). Taken together, these findings suggest that *MSH2* expression is downregulated by stimulation of proinflammatory cytokines through NF-κB activation in human hepatocytes.

TNFα stimulation induces the expression of miR-21 in hepatocytes

To determine whether *MSH2* downregulation induced by TNFα is due to a decrease in transcription or an increase in mRNA degradation, we inhibited *de novo* mRNA synthesis using actinomycin D and evaluated the effect of TNFα treatment on the expression level of *MSH2* mRNA. We found that *MSH2* mRNA levels were significantly reduced by TNFα administration in the presence of actinomycin D, suggesting that *MSH2* downregulation in response to TNFα stimulation is due to increased mRNA degradation in hepatocytes (Fig. 3A). The absence of potential NF-κB–binding sites in the 5′ upstream region of the *MSH2* gene (data not shown), along with the finding that proinflammatory cytokine stimulation increased the degradation of *MSH2* mRNA, led us to hypothesize that miRNAs were involved in the regulation of *MSH2* expression by NF-κB.

Using three representative miRNA target–predicting databases, microRNA.org (http://www.microrna.org), TargetScanHuman 6.2 (http://www.targetscan.org), and MicroCosm Targets Version 5 (http://www.ebi.ac.uk/enright-srv/microcosm/htdocs/targets/v5/), we identified two miRNAs, miR-21 and miR-590-5p, as putative miRNAs that potentially target *MSH2* mRNA *in silico* (Supplementary Fig. S2A). Of the two miRNAs, we focused on miR-21, which has a higher affinity for *MSH2* mRNA than miR-590-5p and is reported to be upregulated in several cancer tissues, including human hepatocellular carcinoma (Fig. 3B; refs. 27, 28).

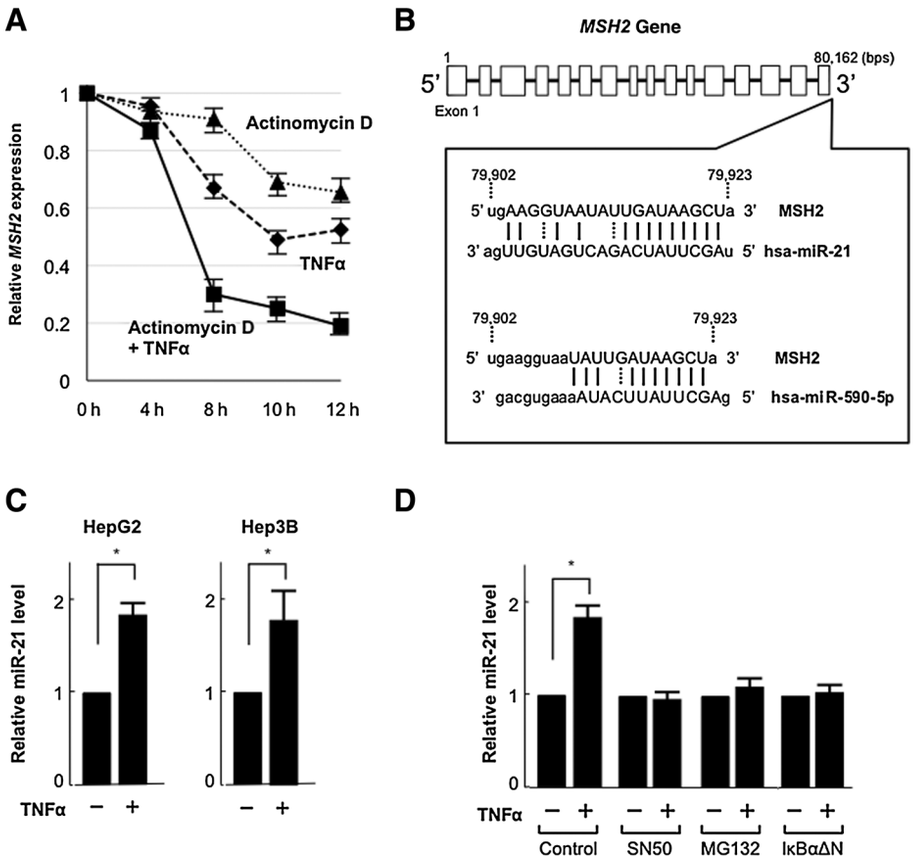

Figure 3.

Expression of miR-21 is induced by TNFα stimulation via NF-κB signaling. **A,** HepG2 cells were treated with actinomycin D, TNFα, or actinomycin D + TNFα. *MSH2* expression levels were measured by quantitative real-time RT-PCR over time (0, 4, 8, 10, and 12 hours). **B,** the predicted miR-21/miR-590-5p–targeting sequence in the 3′-untranslated region of *MSH2* mRNA. **C,** HepG2 and Hep3B cells were treated with TNFα (100 ng/mL) for 8 hours. The miR-21 expression level was significantly increased by TNFα stimulation (*, $P < 0.05$ vs. without TNFα). **D,** HepG2 cells were treated with SN50 (50 μg/mL) or MG132 (2 μg/mL) for 2 hours, or transfected with pcDNA3-IκBαΔN, and further treated with TNFα (100 ng/mL) for 8 hours. The miR-21 expression level was significantly increased by TNFα stimulation when NF-κB activity was not inhibited (*, $P < 0.05$ vs. without TNFα). Total RNA was isolated from each sample, and miR-21 expression levels were measured by TaqMan MicroRNA Assays.

First, we examined miR-21 expression levels in HepG2 and Hep3B cells using TaqMan MicroRNA Assays. miR-21 expression was significantly increased after treatment with TNFα (Fig. 3C). Next, we evaluated whether the increase in miR-21 expression induced by TNFα was mediated by NF-κB activation. Pretreatment with SN50, MG132, or coproduction of the superrepressor form of IκBα almost completely abolished the TNF-α–induced increase in miR-21 expression in HepG2 cells (Fig. 3D). These findings indicate that miR-21 expression is increased by TNFα stimulation through the activation of NF-κB in human hepatocytes.

TNFα-induced downregulation of MSH2 is mediated by miR-21

To examine whether *MSH2* downregulation induced by TNFα is mediated by miR-21 in hepatocytes, expression vectors for miR-21 were transfected into HepG2 and Hep3B cells. Overexpression of miR-21 significantly reduced the expression of both *MSH2* mRNA and MSH2 protein (Fig. 4A and B). To assess the functional consequences of silencing endogenous miR-21 *in vitro*, HepG2 cells infected with a lentivirus vector were used, in which the 3′-untranslated region with three tandem miR-21–binding sequences was linked to the luciferase reporter gene (miR-21 decoy; Supplementary Fig. S2B). When the same amount of control or miR-21 decoy was transduced into HepG2 cells, the luciferase activity was significantly reduced in miR-21 decoy transduced cells (Supplementary Fig. S2C). Transfection of the miR-21 decoy along with the miR-21 expression vector reduced the luciferase activity, whereas transfection of the miR-21 decoy along with an miR-control did not reduce luciferase activity (Supplementary Fig. S2D). TaqMan MicroRNA Assay analysis revealed that the miR-21 level was significantly reduced by expression of the miR-21 decoy (Fig. 4C). Furthermore, expression of the miR-21 decoy restored the TNFα-induced downregulation of both *MSH2* mRNA and MSH2 protein expression (Fig. 4C and D). We further confirmed that miR-21 mediated the *MSH2* downregulation using an anti-miR-21 inhibitor. Expression of miR-21 was significantly reduced, and the TNFα-induced downregulation of both *MSH2* mRNA and MSH2 protein expression was restored by anti-miR-21 inhibitor (Fig. 4E and F).

MSH2 is downregulated and miR-21 is upregulated in human chronic hepatitis tissues

To examine *MSH2* and miR-21 expression in human hepatocytes under physiologic or pathologic conditions, we quantified the *MSH2* transcripts and miR-21 expression levels in human liver tissues with chronic HCV infection and normal liver tissues (Supplementary Fig. S3A). *MSH2* was transcribed in normal liver tissues, with mean *MSH2*/*18s rRNA* ratios of 3.63 ± 2.36 (± SE). On the other hand, HCV-related chronic hepatitis tissues showed significantly lower expression of *MSH2* than that in normal liver tissues (1.75 ± 0.96; Supplementary Fig. S3B). In contrast, there were no significant differences in the expression level of *MSH3*, *MSH6*, *MLH1*, *MLH3*, *PMS1*, or *PMS2* between the liver tissues with and without HCV-related hepatitis, consistent with the findings of human hepatocytes after TNFα treatment (Supplementary Fig. S3C and Fig. 1B). In addition, miR-21 expression in

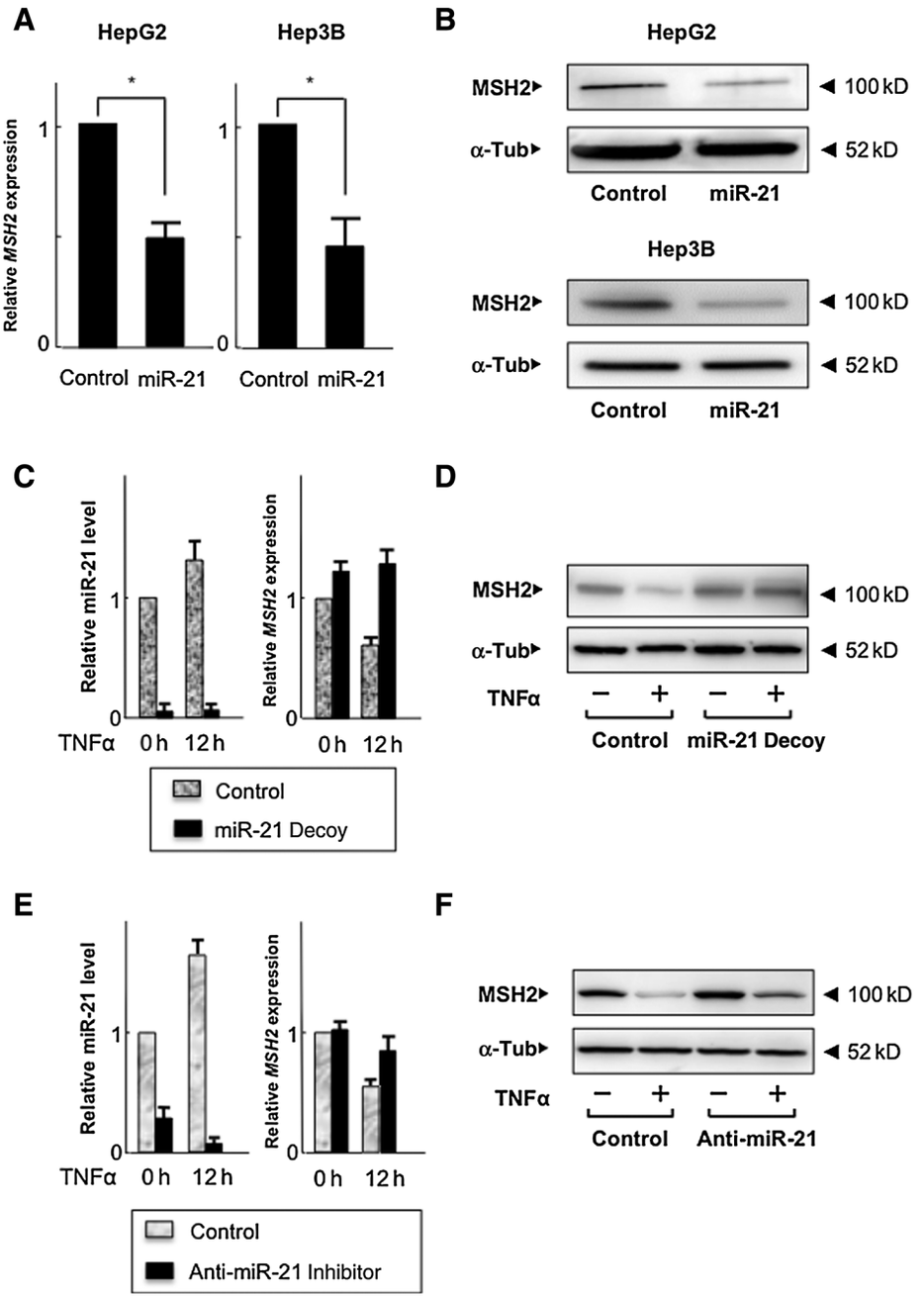

Figure 4.
TNFα-induced downregulation of *MSH2* is mediated by miR-21. **A** and **B,** HepG2 and Hep3B cells were transfected with miR-21 expression vector or control vector. α-Tub, α-tubulin. *MSH2* expression levels were measured by quantitative real-time RT-PCR (**A**; *, $P < 0.05$ vs. control) and immunoblotting, respectively (**B**). **C** and **D,** HepG2 cells were transduced with an miR-21 decoy vector or control vector, followed by TNFα stimulation for 12 hours. miR-21 and *MSH2* expression levels were measured by quantitative real-time RT-PCR (**C**), and MSH2 expression was examined by immunoblotting (**D**). **E** and **F,** HepG2 cells were treated with an anti-miR-21 inhibitor (50 nmol/L) or control for 48 hours and further subjected to TNFα stimulation for 12 hours. miR-21 and *MSH2* expression levels were measured by quantitative real-time RT-PCR (**E**), and MSH2 expression was examined by immunoblotting (**F**).

HCV-related chronic hepatitis tissues was significantly higher than that in normal liver tissues (Supplementary Fig. S3D). Taken together, these findings indicate that TNFα-induced downregulation of *MSH2* transcripts is mediated by miR-21 upregulation in human hepatocytes.

Hepatocellular carcinoma develops in mice with specific disruption of MSH2 and/or AID activation in hepatocytes

Human hepatocellular carcinoma could develop in the liver with chronic inflammation, where *MSH2* downregulation and AID upregulation coexist. Thus, we investigated the phenotypic effects of *MSH2* inactivation and/or AID activation in hepatocytes *in vivo*. To disrupt *MSH2* and/or express AID specifically in the liver, we crossed *MSH2* conditional knockout ($Msh2^{LoxP/LoxP}$) mice (20) and/or AID conditional transgenic (*AID cTg*) mice (21) with transgenic mice carrying a *Cre* gene under control of the albumin (ALB) promoter (*ALB-Cre*; ref. 22). These crosses generated cohorts of mice with various genotypes, including *ALB-Cre*; $Msh2^{LoxP/+}$ (*ALB-MSH2*$^{+/-}$), *ALB-Cre*; $Msh2^{LoxP/LoxP}$ (*ALB-MSH2*$^{-/-}$), *ALB-Cre*; *AID cTg* (*ALB-AID*$^{+}$), *ALB-Cre*; $Msh2^{LoxP/LoxP}$; *AID cTg* (*ALB-MSH2*$^{-/-}$*AID*$^{+}$), *ALB-Cre*, and wild-type (WT) mice. Quantitative RT-PCR and IHC revealed the predicted deletion of MSH2 in the livers of *ALB-MSH2*$^{-/-}$ and *ALB-MSH2*$^{-/-}$*AID*$^{+}$ mice (Fig. 5A and B) and the predicted upregulation of AID in the livers

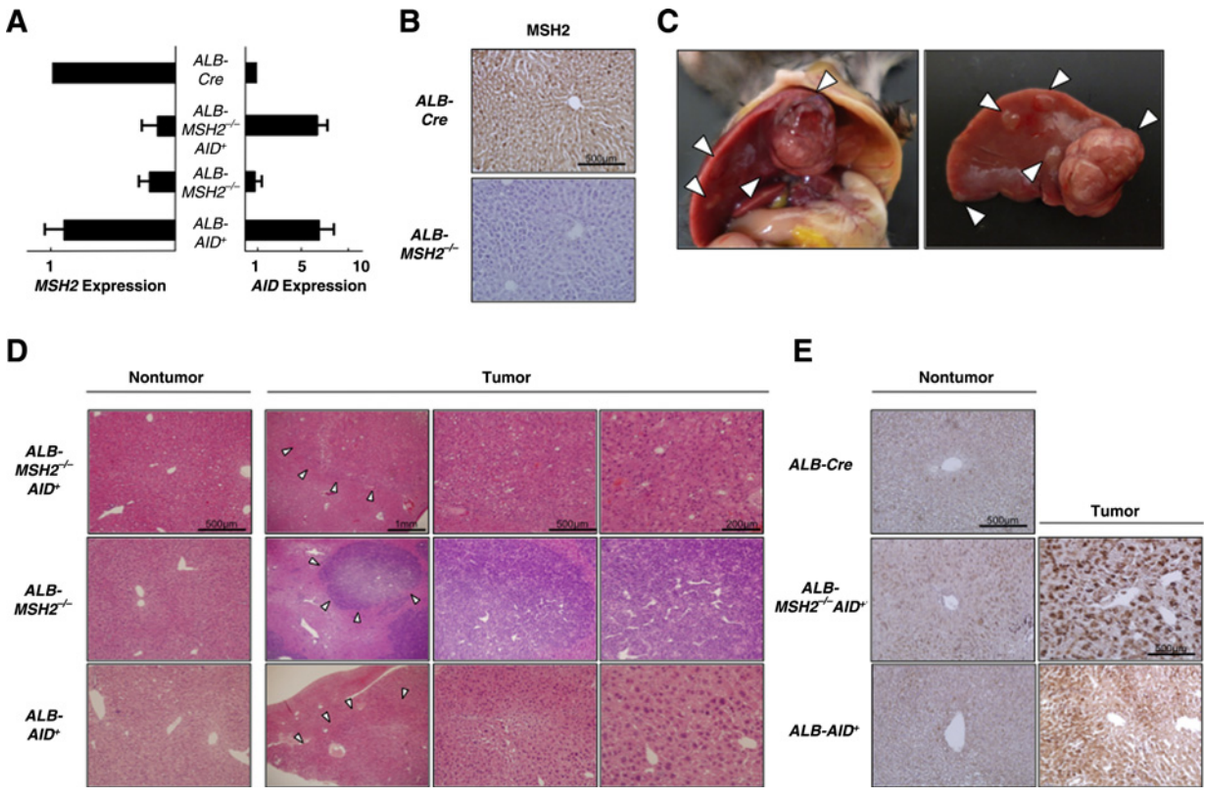

Figure 5.

Liver tumors that developed in *ALB-MSH2*$^{-/-}$*AID*$^{+}$, *ALB-MSH2*$^{-/-}$, and *ALB-AID*$^{+}$ mice. **A** total RNA was isolated from liver tissues of *ALB-Cre, ALB-MSH2*$^{-/-}$*AID*$^{+}$, *ALB-MSH2*$^{-/-}$, and *ALB-AID*$^{+}$ mice, and *MSH2* and AID expression levels were measured by quantitative real-time RT-PCR. **B,** IHC for MSH2 of the *ALB-Cre* and *ALB-MSH2*$^{-/-}$ mouse liver. **C,** representative macroscopic images of multiple liver tumors that developed in an *ALB-MSH2*$^{-/-}$*AID*$^{+}$ mouse. Arrowheads, tumor nodules. **D,** microscopic (hematoxylin and eosin stain) images of liver tumors that developed in *ALB-MSH2*$^{-/-}$*AID*$^{+}$, *ALB-MSH2*$^{-/-}$, and *ALB-AID*$^{+}$ mice and noncancerous liver tissues of the same mice. Arrowheads, tumor nodules. **E,** IHC for α-fetoprotein of nontumor and tumor tissues in *ALB-Cre, ALB-MSH2*$^{-/-}$*AID*$^{+}$, and *ALB-AID*$^{+}$ mice.

of *ALB-AID*$^{+}$ and *ALB-MSH2*$^{-/-}$*AID*$^{+}$ mice (Fig. 5A). *ALB-MSH2*$^{+/-}$, *ALB-MSH2*$^{-/-}$, *ALB-AID*$^{+}$, and *ALB-MSH2*$^{-/-}$*AID*$^{+}$ mice were born alive, appeared healthy, and had a liver weight per body weight ratio comparable with that of *ALB-Cre* mice (data not shown).

Most mice were viable at 90 weeks; however, we frequently observed macroscopic liver tumors in *ALB-MSH2*$^{-/-}$*AID*$^{+}$ mice (Table 1; Fig. 5C). Macroscopic liver tumors developed in 9.1% (1/11) of *ALB-MSH2*$^{+/-}$ and 21.4% (3/14) of *ALB-MSH2*$^{-/-}$ mice at 90 weeks of age, respectively. Notably, liver tumors developed in 23.5% (4/17) of *ALB-AID*$^{+}$ and 50.0% (7/14) of *ALB-MSH2*$^{-/-}$*AID*$^{+}$ mice at 90 weeks of age, indicating that *MSH2* deficiency enhanced the tumorigenesis in the mouse liver with constitutive AID expression. In contrast to these mice, no tumors were observed in *ALB-Cre* and WT mice examined at the same ages. Histologic examination revealed that the tumors of *ALB-MSH2*$^{-/-}$ mice had the characteristics of poorly differentiated hepatocellular carcinoma, and the tumors of *ALB-MSH2*$^{-/-}$*AID*$^{+}$ and *ALB-AID*$^{+}$ mice had the characteristics of well-to-moderately differentiated hepatocellular carcinoma (Fig. 5D). Notably, the expression of α-fetoprotein (AFP), the best-known tumor marker for human hepatocellular carcinoma, was detected in the tumor tissues of *ALB-MSH2*$^{-/-}$*AID*$^{+}$ and *ALB-AID*$^{+}$ mice, whereas no AFP expression was detected in

Table 1. Frequencies of liver tumors observed in each mouse type

Genotype (*n*)	Mean age at sacrificing (weeks)	Liver tumor(s)	
		Frequency	Single/Multiple
ALB-MSH2$^{-/+}$ ($n = 11$)	89.5	9.1% ($n = 1$)	1/0
ALB-MSH2$^{-/-}$ ($n = 14$)	89.1	21.4% ($n = 3$)	1/2
ALB-AID^{+} ($n = 17$)	89.7	23.5% ($n = 4$)	0/4
ALB-MSH2$^{-/-}$*AID*$^{+}$ ($n = 14$)	89.2	50.0% ($n = 7$)	2/5
ALB-Cre ($n = 12$)	88.3	0.0%	—
WT ($n = 10$)	90.0	0.0%	—

Abbreviation: *n*, number of mice.

the nontumorous regions of either mutant or control mouse liver (Fig. 5E). No histologic changes were observed in the nontumorous region of the liver tissues of any of the mutant and control mice examined.

Somatic substitution patterns in MSH2-deficient and/or AID-expressing tumors

To unveil the mutation frequency as well as mutational signature that accumulated in tumors developed in the liver with *MSH2* deficiency and/or AID upregulation, we performed whole-exome sequencing of six hepatocellular carcinomas from *ALB-MSH2*$^{-/-}$*AID*$^{+}$, *ALB-MSH2*$^{-/-}$, and *ALB-AID*$^{+}$ mice. As a control, we also examined the *ALB-Cre* mouse liver. We targeted the whole exons of approximately 24,300 mouse genes, sequenced 1.538 Gb on average for each sample, and achieved 30.04-fold coverage per sample as the mean coverage of each base in the target regions (Supplementary Table S2). The variant filtering process is summarized in Supplementary Fig. S1. Candidate mutations were validated by repeated whole-exome sequencing using independent amplicons derived from the same samples. As a result, we identified a total of 216 single nucleotide variants, including 206 nonsynonymous mutations and 10 synonymous mutations in 121 genes of 6 hepatocellular carcinoma tissues (Supplementary Tables S3 and S4). The number of mutations suggested that MSH2 played a role in protection of AID-mediated mutagenesis in the liver tissues. Among the mutated genes identified, 5, 3, and 6 genes were recurrently mutated in two tumors from *ALB-MSH2*$^{-/-}$*AID*$^{+}$, *ALB-MSH2*$^{-/-}$, and *ALB-AID*$^{+}$ mice, respectively. Pathway analyses using the Kyoto Encyclopedia of Genes and Genomes database (http://www.genome.jp/kegg/) revealed that 6 (*ALB-MSH2*$^{-/-}$*AID*$^{+}$), 9 (*ALB-MSH2*$^{-/-}$), and 6 (*ALB-AID*$^{+}$) genes were categorized into the well-known signaling pathway, whereas the biologic functions of the remaining genes were not fully defined (Supplementary Table S5). Interestingly, several mutated genes such as *Muc6* and *Itga1* were also reported in human liver cancer tissues (International Cancer Genome Consortium; http://icgc.org/).

Accumulating evidence indicates that each cancer has a unique mutational signature (29). We confirmed that the most predominant substitution was C:G to T:A in the exome sequences of hepatocellular carcinomas that developed in *ALB-AID*$^{+}$ mice ($P < 0.05$ by ANOVA; Fig. 6A). In contrast, hepatocellular carcinomas that developed in *ALB-MSH2*$^{-/-}$ mice had unique mutation signatures, with a predominance of T:A to C:G, in addition to C:G to T:A transitions. The mutation signature of hepatocellular carcinomas in *ALB-MSH2*$^{-/-}$*AID*$^{+}$ mice were enriched as C:G to T:A, followed by T:A to C:G (Fig. 6A). Of the 37 C:G to T:A transitions detected in *ALB-MSH2*$^{-/-}$*AID*$^{+}$ mice, 23 (62.2%) were in the context of GpCpX or ApCpX, a typical mutation pattern induced by AID (Fig. 6B). These findings indicate that mutation signatures detected in tumors developing in those models, especially in *ALB-MSH2*$^{-/-}$*AID*$^{+}$ mice, closely resemble those of hepatitis virus–associated human hepatocellular carcinomas, which accumulate somatic mutations biased toward the T:A to C:G and C:G to T:A transition mutations (29, 30).

Discussion

Inflammation is strongly involved in carcinogenesis through various biologic processes. On the other hand, cancer is a genetic disease, and the accumulation of somatic mutations has a crucial role in malignant transformation (31). Therefore, certain mechanisms must facilitate the induction of mutations during inflammation-associated tumor development. Previously, we reported that AID, an APOBEC family protein, plays an important role in the induction of genetic alterations during inflammation-associated cancer development (2). In this study, we demonstrated for the first time that *MSH2* expression is suppressed by TNFα via induction of miR-21 in hepatocytes, which predisposes the inflamed cells to acquire enhanced genetic alterations.

MSH2 is the MMR protein that protects DNA against mutation induction, and its dysfunction is strongly associated with human cancer development (32). Indeed, germline mutation in *MSH2* is the most frequent cause of hereditary nonpolyposis colorectal cancer, known as Lynch syndrome (33). However, little is known about how *MSH2* expression is regulated, except that it is a target gene controlled by the E2F family of transcription factors (34, 35). We showed in this study that TNFα induced downregulation of *MSH2* expression in hepatocytes. The data may be in line with a previous report of the inflammation-mediated epigenetic silencing of *MLH1*, another MMR gene, in the inflamed colonic mucosa (36). Although *PMS2* was upregulated by TNFα stimulation, the biologic implication of *PMS2* upregulation is unclear at present. We also found in this study that transcription factor NF-κB mediates TNFα-induced repression of *MSH2*. NF-κB activation is detected in epithelial cells under inflammatory conditions and strongly involved in inflammation-associated tumorigenesis through various mechanisms, such as regulation of cell survival, proliferation and growth, and epithelial-to-mesenchymal transition (37–40). Our study adds a novel role of NF-κB in inflammation-associated carcinogenesis, namely, suppression of MMR system.

Interestingly, we found in this study that *MSH2* mRNA levels were decreased by TNFα administration even in the presence of actinomycin D, suggesting that *MSH2* downregulation by TNFα is not due to reduced production but is caused by increased degradation of *MSH2* mRNA. These data prompted us to search putative mRNAs that potentially target *MSH2* mRNA, and we identified miR-21, which appeared to have high affinity for *MSH2* mRNA. Consistently, we observed that miR-21 expression was significantly induced by TNFα stimulation via NF-κB activation and that TNFα induced downregulation of *MSH2* mRNA and MSH2 protein expression was restored by an miR-21 decoy or anti-miR-21 inhibitor. The data are in agreement with previous studies showing that miR-21 is transactivated by NF-κB, upregulated in hepatitis livers, and correlating with serum transaminase levels that represent hepatic inflammation activity (41–43). Collectively, our findings indicate that TNFα-induced downregulation of *MSH2* in the setting of inflammation is mediated by NF-κB–induced increase of miR-21 expression. Supporting our idea, the oncogenic property of miR-21 has been demonstrated in various tumors. For example, miR-21 is upregulated in various solid tumors, and its expression levels are closely correlated with the aggressive form and poor prognosis of several tumors, such as breast and lung cancers (44, 45).

In this study, using transgenic mouse models, we observed that hepatocyte-specific loss of *MSH2* results in the development of liver tumors with features of hepatocellular carcinoma. Indeed, 21.4% of *ALB-MSH2*$^{-/-}$ mice developed tumors in the liver. Notably, the incidence of tumor development in AID-expressing liver was substantially augmented by *MSH2* deficiency (50.0% in *ALB-MSH2*$^{-/-}$*AID*$^{+}$ mice vs. 23.5% in *ALB-AID*$^{+}$ mice).

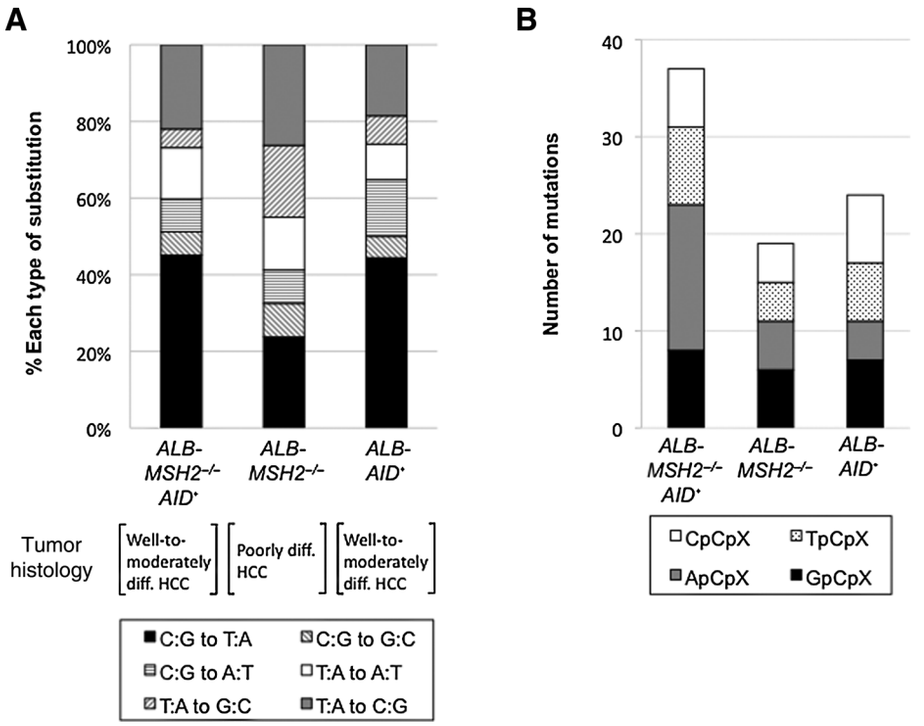

Figure 6.
Somatic mutation patterns in liver tumors of *ALB-MSH2*$^{-/-}$*AID*$^{+}$, *ALB-MSH2*$^{-/-}$, and *ALB-AID*$^{+}$ mice. **A,** the mutational signature determined by the whole-exome sequences of six independent tumors in total from *ALB-MSH2*$^{-/-}$*AID*$^{+}$, *ALB-MSH2*$^{-/-}$, and *ALB-AID*$^{+}$ mice. The mutational signature in *ALB-MSH2*$^{-/-}$*AID*$^{+}$ mice was enriched as C:G to T:A, followed by T:A to C:G. Well-to-moderately diff. HCC, well-to-moderately differentiated hepatocellular carcinoma; poorly diff. HCC, poorly differentiated hepatocellular carcinoma. **B,** sequence context of the C:G to T:A transitions in *ALB-MSH2*$^{-/-}$*AID*$^{+}$, *ALB-MSH2*$^{-/-}$, and *ALB-AID*$^{+}$ mice liver tumor tissues. GpCpX and ApCpX patterns were enriched in *ALB-MSH2*$^{-/-}$*AID*$^{+}$ mice.

Moreover, whole-exome sequencing analyses revealed that mutation frequency was increased in the tumor tissues of *ALB-MSH2*$^{-/-}$*AID*$^{+}$ mice as compared with that in *ALB-AID*$^{+}$ mice. Interestingly, somatic substitution signatures accumulated in the tumors that developed in *ALB-MSH2*$^{-/-}$*AID*$^{+}$ mice had predominantly C:G to T:A transitions. The preferential bias to C:G to T:A transitions at the preferred AID target sequence, that is, GpCpX or ApCpX trinucleotides enriched in the tumors of *ALB-MSH2*$^{-/-}$*AID*$^{+}$ mice suggest that *MSH2* is required for protection of AID-mediated mutagenesis, and dysfunction of *MSH2* concurrent with AID expression strongly accelerates tumorigenesis in liver tissues.

In addition to a predominance of C:G to T:A transitions in *ALB-MSH2*$^{-/-}$*AID*$^{+}$ mice tumors, whole-exome sequencing revealed a predominance of T:A to C:G transitions in *ALB-MSH2*$^{-/-}$ mice tumors and increase of T:A to C:G transitions in *ALB-MSH2*$^{-/-}$*AID*$^{+}$ mice tumors as compared with those in *ALB-AID*$^{+}$ mice. Our data are in agreement with a previous study of MMR-deficient mice showing that the mutations accumulated in the reporter gene of epithelial cells of *MSH2*-deficient mice are biased toward T:A to C:G mutations (46). A recent deep sequencing analysis also revealed that a yeast strain with MSH2 dysfunction accumulates somatic mutations biased toward the transition mutations, T:A to C:G and C:G to T:A substitutions (47). Moreover, whole-genome sequencing on MMR-deficient human tumors also revealed that approximately 3 of 4 of all nucleotide substitutions represent transition mutations, including T:A to C:G and C:G to T:A (48). Importantly, T:A to C:G transitions are enriched in human hepatocellular carcinoma tissues (30). In this study, we showed the reduced expression of *MSH2* in human chronic hepatitis tissues with HCV infection. Taken together, it is tempting to speculate that *MSH2* dysfunction is involved in inflammation-associated carcinogenesis in human liver. The reason why *MSH2* deficiency preferentially induces T:A to C:G transition remains unknown.

In conclusion, we found in this study that *MSH2* expression was downregulated by TNFα via NF-κB–mediated miR-21 expression in hepatocytes and that these mechanisms may contribute to inflammation-associated hepatocarcinogenesis through enhanced susceptibility to mutagenesis. Previously, we reported an important role of AID in promoting gene mutations during inflammation-associated carcinogenesis (2). Thus, inflammation appears to enhance genetic alteration by not only accelerating gene mutation induction but also inhibiting MMR, both of which are working in concert, leading to cancer development.

Disclosure of Potential Conflicts of Interest

No potential conflicts of interest were disclosed.

Authors' Contributions

Conception and design: Y. Eso, T. Chiba, H. Marusawa
Development of methodology: Y. Eso, H. Marusawa
Acquisition of data (provided animals, acquired and managed patients, provided facilities, etc.): Y. Eso, T. Inuzuka, K. Lee, W. Edelmann, H. Marusawa
Analysis and interpretation of data (e.g., statistical analysis, biostatistics, computational analysis): Y. Eso, T. Matsumoto, T. Inuzuka, H. Marusawa
Writing, review, and/or revision of the manuscript: Y. Eso, A. Takai, W. Edelmann, H. Marusawa
Administrative, technical, or material support (i.e., reporting or organizing data, constructing databases): Y. Eso, T. Inuzuka, T. Horie, K. Ono, S. Uemoto, H. Marusawa
Study supervision: H. Marusawa

Acknowledgments

The authors thank Dr. T. Honjo for his generous gift of *AID cTg* mice. The authors also thank Drs. K. Takahashi and Y. Ueda for helpful suggestions and Drs. S. K. Kim, T. Shimizu, and Y. Matsumoto for help with the analysis.

Grant Support

This work was supported by the Japan Society for the Promotion of Science (JSPS) Grants-in-Aid for Scientific Research, KAKENHI (26293172), and the Research Program on Hepatitis from Japan Agency for Medical Research and Development, AMED, Japan, and NIH grants (CA76329 and CA13330).

The costs of publication of this article were defrayed in part by the payment of page charges. This article must therefore be hereby marked *advertisement* in accordance with 18 U.S.C. Section 1734 solely to indicate this fact.

Received October 24, 2015; revised April 28, 2016; accepted May 4, 2016; published OnlineFirst June 3, 2016.

References

1. Coussens LM, Werb Z. Inflammation and cancer. Nature 2002;420:860–7.
2. Chiba T, Marusawa H, Ushijima T. Inflammation-associated cancer development in digestive organs: mechanisms and roles for genetic and epigenetic modulation. Gastroenterology 2012;143:550–63.
3. Lengauer C, Kinzler KW, Vogelstein B. Genetic instabilities in human cancers. Nature 1998;396:643–9.
4. Hanahan D, Weinberg RA. The hallmarks of cancer. Cell 2000;100:57–70.
5. Loeb LA, Bielas JH, Beckman RA. Cancers exhibit a mutator phenotype: clinical implications. Cancer Res 2008;68:3551–7.
6. Ikeda A, Shimizu T, Matsumoto Y, Fujii Y, Eso Y, Inuzuka T, et al. Leptin receptor somatic mutations are frequent in HCV-infected cirrhotic liver and associated with hepatocellular carcinoma. Gastroenterology 2014;146:222–32.
7. Shimizu T, Marusawa H, Matsumoto Y, Inuzuka T, Ikeda A, Fujii Y, et al. Accumulation of somatic mutations in TP53 in gastric epithelium with *Helicobacter pylori* infection. Gastroenterology 2014;147:407–17.
8. Weaver JM, Ross-Innes CS, Shannon N, Lynch AG, Forshew T, Barbera M, et al. Ordering of mutations in preinvasive disease stages of esophageal carcinogenesis. Nat Genet 2014;46:837–43.
9. Roberts SA, Gordenin DA. Hypermutation in human cancer genomes: footprints and mechanisms. Nat Rev Cancer 2014;14:786–800.
10. Roberts SA, Lawrence MS, Klimczak LJ, Grimm SA, Fargo D, Stojanov P, et al. An APOBEC cytidine deaminase mutagenesis pattern is widespread in human cancers. Nat Genet 2013;45:970–6.
11. Swanton C, McGranahan N, Starrett GJ, Harris RS. APOBEC enzymes: mutagenic fuel for cancer evolution and heterogeneity. Cancer Discov 2015;5:704–12.
12. Honjo T, Kinoshita K, Muramatsu M. Molecular mechanism of class switch recombination: linkage with somatic hypermutation. Annu Rev Immunol 2002;20:165–96.
13. Kou T, Marusawa H, Kinoshita K, Endo Y, Okazaki IM, Ueda Y, et al. Expression of activation-induced cytidine deaminase in human hepatocytes during hepatocarcinogenesis. Int J Cancer 2007;120:469–76.
14. Endo Y, Marusawa H, Kinoshita K, Morisawa T, Sakurai T, Okazaki IM, et al. Expression of activation-induced cytidine deaminase in human hepatocytes via NF-kappaB signaling. Oncogene 2007;26:5587–95.
15. Matsumoto Y, Marusawa H, Kinoshita K, Endo Y, Kou T, Morisawa T, et al. *Helicobacter pylori* infection triggers aberrant expression of activation-induced cytidine deaminase in gastric epithelium. Nat Med 2007;13:470–6.
16. Matsumoto Y, Marusawa H, Kinoshita K, Niwa Y, Sakai Y, Chiba T. Upregulation of activation-induced cytidine deaminase causes genetic aberrations at the CDKN2b-CDKN2a in gastric cancer. Gastroenterology 2010;139:1984–94.
17. Endo Y, Marusawa H, Kou T, Nakase H, Fujii S, Fujimori T, et al. Activation-induced cytidine deaminase links between inflammation and the development of colitis-associated colorectal cancers. Gastroenterology 2008;135:889–98.
18. Liu M, Duke JL, Richter DJ, Vinuesa CG, Goodnow CC, Kleinstein SH, et al. Two levels of protection for the B cell genome during somatic hypermutation. Nature 2008;451:841–5.
19. Phung QH, Winter DB, Cranston A, Tarone RE, Bohr VA, Fishel R, et al. Increased hypermutation at G and C nucleotides in immunoglobulin variable genes from mice deficient in the MSH2 mismatch repair protein. J Exp Med 1998;187:1745–51.
20. Kucherlapati MH, Lee K, Nguyen AA, Clark AB, Hou H, Rosulek A, et al. An Msh2 conditional knockout mouse for studying intestinal cancer and testing anticancer agents. Gastroenterology 2010;138:993–1002.
21. Muto T, Okazaki IM, Yamada S, Tanaka Y, Kinoshita K, Muramatsu M, et al. Negative regulation of activation-induced cytidine deaminase in B cells. Proc Natl Acad Sci USA 2006;103:2752–7.
22. Aoi T, Yae K, Nakagawa M, Ichisaka T, Okita K, Takahashi K, et al. Generation of pluripotent stem cells from adult mouse liver and stomach cells. Science 2008;321:699–702.
23. Tilg H, Wilmer A, Vogel W, Herold M, Nölchen B, Judmaier G, et al. Serum levels of cytokines in chronic liver diseases. Gastroenterology 1992;103:264–74.
24. González-Amaro R, García-Monzón C, García-Buey L, Moreno-Otero R, Alonso JL, Yagüe E, et al. Induction of tumor necrosis factor alpha production by human hepatocytes in chronic viral hepatitis. J Exp Med 1994;179:841–8.
25. Larrea E, Garcia N, Qian C, Civeira MP, Prieto J. Tumor necrosis factor alpha gene expression and the response to interferon in chronic hepatitis C. Hepatology 1996;23:210–7.
26. Karin M, Lin A. NF-kappaB at the crossroads of life and death. Nat Immunol 2002;3:221–7.
27. Volinia S, Calin GA, Liu CG, Ambs S, Cimmino A, Petrocca F, et al. A microRNA expression signature of human solid tumors defines cancer gene targets. Proc Natl Acad Sci U S A 2006;103:2257–61.
28. Tili E, Michaille JJ, Croce CM. MicroRNAs play a central role in molecular dysfunctions linking inflammation with cancer. Immunol Rev 2013;253:167–84.
29. Alexandrov LB, Nik-Zainal S, Wedge DC, Aparicio SA, Behjati S, Biankin AV, et al. Signatures of mutational processes in human cancer. Nature 2013;500:415–21.
30. Totoki Y, Tatsuno K, Yamamoto S, Arai Y, Hosoda F, Ishikawa S, et al. High-resolution characterization of a hepatocellular carcinoma genome. Nat Genet 2011;43:464–9.
31. Vogelstein B, Kinzler KW. Cancer genes and the pathways they control. Nat Med 2004;10:789–99.
32. Jiricny J. The multifaceted mismatch-repair system. Nat Rev Mol Cell Biol 2006;7:335–46.
33. Fishel R, Lescoe MK, Rao MR, Copeland NG, Jenkins NA, Garber J, et al. The human mutator gene homolog MSH2 and its association with hereditary nonpolyposis colon cancer. Cell 1993;75:1027–38.
34. Polager S, Kalma Y, Berkovich E, Ginsberg D. E2Fs up-regulate expression of genes involved in DNA replication, DNA repair and mitosis. Oncogene 2002;21:437–46.
35. Ren B, Cam H, Takahashi Y, Volkert T, Terragni J, Young RA, et al. E2F integrates cell cycle progression with DNA repair, replication, and G(2)/M checkpoints. Genes Dev 2002;16:245–56.
36. Edwards RA, Witherspoon M, Wang K, Afrasiabi K, Pham T, Birnbaumer L, et al. Epigenetic repression of DNA mismatch repair by inflammation and hypoxia in inflammatory bowel disease-associated colorectal cancer. Cancer Res 2009;69:6423–9.
37. Pikarsky E, Porat RM, Stein I, Abramovitch R, Amit S, Kasem S, et al. NF-kappaB functions as a tumour promoter in inflammation-associated cancer. Nature 2004;431:461–6.
38. Ben-Neriah Y, Karin M. Inflammation meets cancer, with NF-κB as the matchmaker. Nat Immunol 2011;12:715–23.
39. Viala J, Chaput C, Boneca IG, Cardona A, Girardin SE, Moran AP, et al. Nod1 responds to peptidoglycan delivered by the *Helicobacter pylori* cag pathogenicity island. Nat Immunol 2004;5:1166–74.
40. Li CW, Xia W, Huo L, Lim SO, Wu Y, Hsu JL, et al. Epithelial-mesenchymal transition induced by TNF-α requires NF-κB-mediated transcriptional upregulation of Twist1. Cancer Res 2012;72:1290–300.

41. Jiang J, Gusev Y, Aderca I, Mettler TA, Nagorney DM, Brackett DJ, et al. Association of microRNA expression in hepatocellular carcinomas with hepatitis infection, cirrhosis, and patient survival. Clin Cancer Res 2008;14:419–27.
42. Marquez RT, Bandyopadhyay S, Wendlandt EB, Keck K, Hoffer BA, Icardi MS, et al. Correlation between microRNA expression levels and clinical parameters associated with chronic hepatitis C viral infection in humans. Lab Invest 2010;90:1727–36.
43. Sheedy FJ, Palsson-McDermott E, Hennessy EJ, Martin C, O'Leary JJ, Ruan Q, et al. Negative regulation of TLR4 via targeting of the proinflammatory tumor suppressor PDCD4 by the microRNA miR-21. Nat Immunol 2010;11:141–7.
44. Yan LX, Huang XF, Shao Q, Huang MY, Deng L, Wu QL, et al. MicroRNA miR-21 overexpression in human breast cancer is associated with advanced clinical stage, lymph node metastasis and patient poor prognosis. RNA 2008;14:2348–60.
45. Saito M, Schetter AJ, Mollerup S, Kohno T, Skaug V, Bowman ED, et al. The association of microRNA expression with prognosis and progression in early-stage, non-small cell lung adenocarcinoma: a retrospective analysis of three cohorts. Clin Cancer Res 2011;17:1875–82.
46. Hegan DC, Narayanan L, Jirik FR, Edelmann W, Liskay RM, Glazer PM. Differing patterns of genetic instability in mice deficient in the mismatch repair genes Pms2, Mlh1, Msh2, Msh3 and Msh6. Carcinogenesis 2006;27:2402–8.
47. Lang GI, Parsons L, Gammie AE. Mutation rates, spectra, and genome-wide distribution of spontaneous mutations in mismatch repair deficient yeast. G3 2013;3:1453–65.
48. Zhao H, Thienpont B, Yesilyurt BT, Moisse M, Reumers J, Coenegrachts L, et al. Mismatch repair deficiency endows tumors with a unique mutation signature and sensitivity to DNA double-strand breaks. eLife 2014;3:e02725.